

Switching of valley polarization and topology in twisted bilayer graphene by electric currents

Ying Su¹ and Shi-Zeng Lin¹

¹*Theoretical Division, T-4 and CNLS, Los Alamos National Laboratory, Los Alamos, New Mexico 87545, USA*
(Dated: December 21, 2024)

It is observed experimentally that the sign of the Hall resistance can be flipped by a dc electric current in the twisted bilayer graphene (TBG) at 3/4 filling of the four-fold degenerate conduction flat bands. The experiment implies a switching of the valley polarization (VP) and topology in TBG. Here we present a theory on the current-induced switching of VP and topology. The presence of current in the bulk causes the redistribution of electron occupation in bands near the Fermi energy, which then deforms and shifts the band dispersion due to the Coulomb interaction. Above a critical current, the original occupied and empty bands can be swapped resulting in the switching of VP and topology.

Introduction.—The electronic band structure is modified significantly compared to that in a single layer graphene, when two layers of graphene are stacked together [1]. The bandwidth can be controlled by the misalignment angle between two layers [2, 3]. At certain twisted angles called magic angles, the energy bands near the Fermi surface are extremely flat [3], where the Coulomb interaction becomes dominant over the kinetic energy of electrons. It is expected that novel quantum states enabled by the strong electronic correlation will emerge. Indeed, the correlated insulating state and superconductivity have been observed experimentally in the magic-angle twisted bilayer graphene (TBG) [4, 5]. Furthermore, the insulating state can have nontrivial topology which is manifested by the intrinsic quantum anomalous Hall effect (QAHE) [6, 7]. The twisted multilayer graphene therefore becomes an important platform to explore the physics of strong electronic correlation and topology [4–76].

The QAHE with orbital ferromagnetism was observed at 3/4 filling of the upper flat bands in TBG recently [6, 7]. In the absence of electronic interaction, the electronic bands of TBG have the four-fold degeneracy associated with the valley and spin degrees of freedom. The strong electronic interaction in flat bands lifts the valley and spin degeneracy, that results in the valley-spin-polarized insulating state responsible for the QAHE at 3/4 filling [19, 57, 69–72]. The nontrivial topology of the insulating state is characterized by the Chern number $C = \pm 1$, where the sign of Chern number depends on which valley is polarized. Remarkably, as demonstrated in experiments, the sign of Hall conductance can be flipped by a dc current, that indicates the switching of Chern number and valley polarization (VP) [6, 7]. It is argued that the orbital magneto-electric effect is responsible for the switching of Chern number by currents [48]. It is also suggested that the asymmetric edges of TBG can result in the free energy difference for the chiral edge currents in opposite directions [7]. However, to change the topology, it is required to overcome a bulk energy barrier, that increases linearly with volume of the system. It is unclear whether an edge current alone is sufficient to overcome the bulk energy barrier. [77].

In this paper, we propose a mechanism of switching of VP and Chern number in TBG by electric currents in the bulk. The current causes the redistribution of the electron occupa-

tion in otherwise fully occupied or empty bands, which deforms and shifts the band dispersion with respect to the Fermi energy E_F due to the Coulomb interaction. Above a threshold current, the major part of the originally empty (occupied) band when current is absent is pushed below (above) E_F . The bands then are swapped after relaxation when the current is removed, that hence results in flipping of the VP and topology.

Toy model.—To facilitate the understanding of switching of VP by electric currents, we use a simple toy model to demonstrate the physical picture. Here we consider a two-band model described by the Hamiltonian

$$\mathcal{H} = \sum_{k,\tau} (\varepsilon_{k,\tau} - \lambda \partial_k \varepsilon_{k,\tau}) c_{k,\tau}^\dagger c_{k,\tau} + V \sum_{k_1, k_2} c_{k_1,+}^\dagger c_{k_1,+} c_{k_2,-}^\dagger c_{k_2,-}, \quad (1)$$

where $\tau = \pm$ is the effective valley index labeling the two energy bands and V is the repulsive intervalley interaction. The model has time-reversal symmetry (TRS), $\varepsilon_{k,\tau} = \varepsilon_{-k,-\tau}$. The current in the system can be introduced by the Lagrangian multiplier λ , which has the meaning of electric field times electron lifetime times electric charge according to the semiclassical Boltzmann transport theory. Thus $\lambda \partial_k \varepsilon_{k,\tau}$ becomes the energy gain of electrons in the presence of an electric field. The corresponding self-consistent mean-field Hamiltonian is $\mathcal{H}_{MF} = \sum_{k,\tau} E_{k,\tau} c_{k,\tau}^\dagger c_{k,\tau}$ with $E_{k,\tau} = \varepsilon_{k,\tau} - \lambda \partial_k \varepsilon_{k,\tau} + \Delta_{-\tau}$ and $\Delta_{\tau} = V \sum_k f(E_{k,\tau})$, where $f(E_{k,\tau})$ is the Fermi distribution function.

Consider the schematic band dispersions shown in Fig. 1(a). The band with valley + is above that with valley – as a consequence of the spontaneous symmetry breaking due to the intervalley interaction. The system is an insulator at half filling. To introduce current, a fraction of electrons in the lower band must be pumped into the upper band. Because the electron self-energy depends on the electron occupation, the part of – band with group velocity opposite to the current direction rises while the + band shifts downwards. The majority of the + band can be below the – band above a critical current, as shown in Fig. 1(b). In this circumstance and after removing the current, the system relaxes into a state with + (–) band occupied (empty), and thus the VP is switched, as shown in Fig. 1(c).

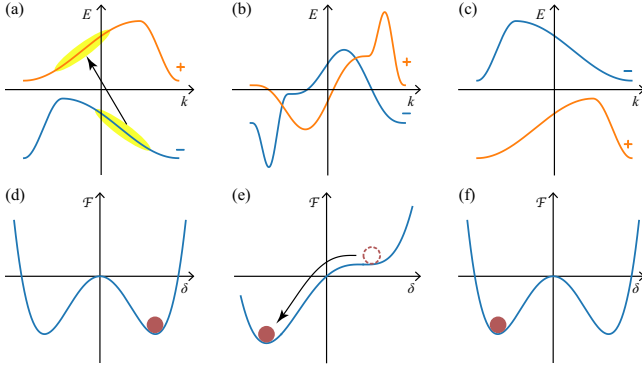


FIG. 1. (a)-(c) Schematic band structures for $\lambda = 0$, $\lambda \geq \lambda_c$, and $\lambda = 0$, respectively. (d)-(f) Free energy profiles correspond to (a)-(c). The two energy bands are labeled by the effective valley index \pm . (a) and (c) represent the two degenerate ground states with opposite VP. (b) is obtained from (a) by introducing the current, and (c) is obtained from (b) by removing the current. The current induced pumping of electrons from the lower band to the upper band is indicated by the arrow and is highlighted in (a). The switching of VP and vanishing of energy barrier in the presence of current is exhibited in (e).

To describe the phase transition associated with the switching of VP, we introduce the VP order parameter $\delta = (\Delta_+ - \Delta_-)/2$. Close to the transition temperature T_c when δ is small, the Ginzburg-Landau free energy of the system can be expanded as [77]

$$\mathcal{F} = \mathcal{F}_0 + \alpha_1 \delta + \alpha_2 \delta^2 + \alpha_3 \delta^3 + \alpha_4 \delta^4. \quad (2)$$

Because both current and δ are odd under time reversal, it requires $\alpha_{1,3}(\lambda) = -\alpha_{1,3}(-\lambda)$ and $\alpha_{2,4}(\lambda) = \alpha_{2,4}(-\lambda)$. Under the inversion operation *within* each valley $\hat{\Gamma}_v$, i.e. $\varepsilon_{k,\tau} \rightarrow \varepsilon_{-k,\tau}$, δ is even while the current is odd. If the system has the symmetry associated with $\hat{\Gamma}_v$, then $\alpha_{1,3}(\lambda) = \alpha_{1,3}(-\lambda)$, which immediately implies $\alpha_{1,3}(\lambda) = 0$. Therefore this intravalley inversion symmetry must be broken, i.e. $\varepsilon_{k,\tau} \neq \varepsilon_{-k,\tau}$, in order to make the current-induced switching of valley polarization possible.

It is clear from Eq. (2) that the system has two degenerate ground states with opposite VP, which are separated by an energy barrier, as shown in Figs. 1(d) and 1(f). The presence of current lifts the degeneracy by increasing the energy of one valley-polarized state and reducing the energy of the other one, as shown in Fig. 1(e). Above a critical current, the energy barrier vanishes. The VP of the system is switched if it is initiated at a state, that becomes unstable under the current [see Fig. 1(e)]. On the other hand, if the system sits in the other state that remains the energy minimal under the current, there is no switching of VP. Thus the switching of VP depends on the direction of current.

TBG.—We then apply our physical picture to TBG with a small twist angle. In TBG, no symmetry guarantees $\varepsilon_{k,\tau} = \varepsilon_{-k,\tau}$ and therefore it is possible to switch the VP by electric

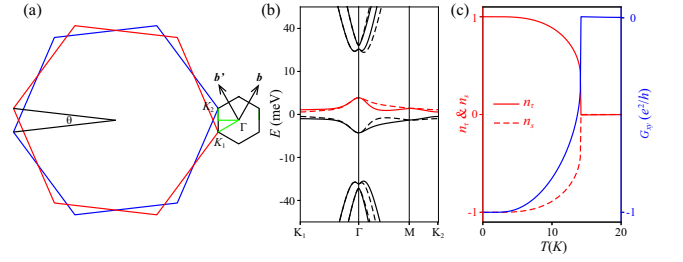


FIG. 2. (a) Schematic BZs of the TBG (black hexagon) and of two graphene layers (red and blue hexagons). (b) Low-energy band structure of the TBG along the high symmetry path. The solid and dashed energy bands are from the $\pm K$ valleys, respectively. The upper flat bands are marked by red color. (c) n_τ (red solid line), n_s (red dashed line), and Hall conductance G_{xy} (blue solid line) are plotted as a function of the temperature T .

currents. We employ the continuum model Hamiltonian [3]

$$\mathcal{H}_{k,\tau} = \begin{pmatrix} h_{1,\tau}(\mathbf{k}) & T_\tau(\mathbf{r}) \\ T_\tau^\dagger(\mathbf{r}) & h_{2,\tau}(\mathbf{k}) \end{pmatrix}, \quad (3)$$

where $\tau = \pm$ is the valley index and $h_{l,\tau}(\mathbf{k})$ is the low-energy effective Dirac Hamiltonian of the l -th layer graphene. Under the twist that the first (second) layer is rotated by $\theta/2$ ($-\theta/2$), the Dirac Hamiltonian becomes

$$h_{l,\tau}(\mathbf{k}) = \mathcal{R}(\pm\tau\theta/2) \hbar v_F (\mathbf{k} - \tau \mathbf{K}_l) \cdot \boldsymbol{\sigma}_\tau \mathcal{R}(\pm\tau\theta/2)^{-1}, \quad (4)$$

where $\mathcal{R}(\theta) = e^{-i\theta\sigma_z/2}$ is the rotation operator and $\boldsymbol{\sigma}_\tau = (\tau\sigma_x, \sigma_y)$ is the Pauli matrix for sublattice degree of freedom. \mathbf{K}_l are the corners of Moiré Brouillon zone (BZ) as shown in Fig. 2(a). The interlayer coupling is described by

$$T_\tau(\mathbf{r}) = T_\tau^{(0)} + e^{-i\tau\mathbf{b}\cdot\mathbf{r}} T_\tau^{(1)} + e^{-i\tau\mathbf{b}'\cdot\mathbf{r}} T_\tau^{(2)}, \quad (5)$$

$$T_\tau^{(n)} = w_{AA}\sigma_0 + w_{AB} \cos\left(\frac{2\pi n}{3}\right) \sigma_x + \tau w_{AB} \sin\left(\frac{2\pi n}{3}\right) \sigma_y,$$

where \mathbf{b} (\mathbf{b}') are the primitive reciprocal lattice vectors of the TBG [see Fig. 2(a)]. Due to the lattice relaxation, the interlayer tunneling strength is different for the AA and AB stacking regions, where $w_{AA} = 79.7$ meV and $w_{AB} = 97.5$ meV [12]. The Fermi velocity is $\hbar v_F/a = 2.1354$ eV where $a = 0.246$ nm is the lattice constant of single layer graphene. $\mathcal{H}_{k,\pm}$ of the $\pm K$ valleys are related by TRS. In the experiment, the TBG with $\theta = 1.15^\circ$ is aligned with a hBN substrate that induces a sublattice potential onto the first layer graphene as $h_{1,\tau} \rightarrow h_{1,\tau} + \Delta_{AB}\sigma_z/2$ [7]. We choose the sublattice potential $\Delta_{AB} = 20$ meV in this study. The low-energy bands of the TBG are shown in Fig. 2(b), where the energy bands from the $\pm K$ valley are represented by solid and dashed lines, respectively. There are eight flat bands including the degenerate spin degree of freedom around zero energy. The lattice relaxation isolates the flat bands from remotes bands and the sublattice potential induced by the substrate gaps the upper flat bands from the lower flat bands.

Here we focus on the 3/4 filling of the upper flat bands [the red bands in Fig. 2(b)], where the QAHE emerges [6, 7]. By projecting the Coulomb interaction onto the upper flat bands, the Hamiltonian of TBG becomes

$$\mathcal{H}_0 = \sum_{k,\tau,s} (\varepsilon_{k,\tau} - \mu) c_{k,\tau,s}^\dagger c_{k,\tau,s} + \frac{1}{2A} \sum_q \rho(q) V(q) \rho(-q), \quad (6)$$

where $\varepsilon_{k,\tau}$ denotes the spin-degenerate bare dispersion for the upper flat bands given by $\mathcal{H}_{k,\tau} |\psi_{k,\tau}\rangle = \varepsilon_{k,\tau} |\psi_{k,\tau}\rangle$, μ is the chemical potential, and A is the area of the system. $s = \uparrow$ or \downarrow represents the spin degree of freedom. $\rho(q) = \sum_{k,k',\tau,s} \langle \psi_{k,\tau} | e^{iq \cdot r} | \psi_{k',\tau} \rangle c_{k,\tau,s}^\dagger c_{k',\tau,s}$ is the density operator, and $V(q) = e^2 \tanh(|q|d)/2\epsilon|q|$ is the screened Coulomb potential, where ϵ is the dielectric constant and d is the distance between TBG and metallic gates. Here we take $d = 40$ nm following the experiment [7].

With the self-consistent Hartree-Fock approximation, the dispersion of the upper flat bands are corrected by the Coulomb interaction as

$$\begin{aligned} E_{k,\tau,s} &= \varepsilon_{k,\tau} - \mu \\ &+ \frac{1}{A} \sum_{q,k',\tau',s'} \langle \psi_{k,\tau} | e^{iq \cdot r} | \psi_{k',\tau'} \rangle V(q) \langle \psi_{k',\tau'} | e^{-iq \cdot r} | \psi_{k',\tau'} \rangle f(E_{k',\tau',s'}) \\ &- \frac{1}{A} \sum_{q,k'} \langle \psi_{k,\tau} | e^{iq \cdot r} | \psi_{k',\tau'} \rangle V(q) \langle \psi_{k',\tau'} | e^{-iq \cdot r} | \psi_{k,\tau} \rangle f(E_{k',\tau,s}) \end{aligned} \quad (7)$$

By solving the self-consistent equation, we get four degenerate valley-spin-polarized ground states at 3/4 filling. In the ground states, one of the four flat bands is above the other three that results in an insulating state. The experimentally measured energy gap is $\Delta/k_B \approx 27$ K [7], that can be reproduced by our approach with $\epsilon = 58.6\epsilon_0$, where ϵ_0 is the vacuum permittivity.

We define $n_\tau = \sum_s (n_{+,s} - n_{-,s})$ and $n_s = \sum_\tau (n_{\tau,\uparrow} - n_{\tau,\downarrow})$ to characterize the valley and spin polarization, respectively. $n_{\tau,s}$ is the occupation number of the flat band with the valley-spin indices (τ, s) . We consider a symmetry-breaking state with $n_\tau = -n_s = 1$ at zero temperature, as shown in Fig. 3. The four flat bands have nonzero Chern numbers $C = \pm 1$, which are opposite for $\pm K$ valleys as a consequence of TRS. Therefore, the VP at 3/4 filling ensures the QAHE, which is manifested by the quantized Hall conductance $G_{xy} = \pm e^2/h$ in experiments [7]. Because the Hamiltonian Eq. (6) has the spin SU(2) symmetry and valley U(1) symmetry, the long-range spin order is destroyed by thermal fluctuations according to the Mermin-Wagner theorem, while the long-range valley order is allowed [78]. As temperature increases, the mean field n_τ , n_s , and G_{xy} vanish together above a critical temperature $T_c = 14.1$ K. [see Fig. 2(c)]

We then study the effect of current and magnetic field on the electron dispersion. The current is introduced through the Lagrange multiplier as before and the Hamiltonian becomes

$$\mathcal{H} = \mathcal{H}_0 - \sum_{k,\tau,s} (\lambda_s \partial_{k_x} \varepsilon_{k,\tau} + g\mu_B s_z B + M_{k,\tau} B) c_{k,\tau,s}^\dagger c_{k,\tau,s}, \quad (8)$$

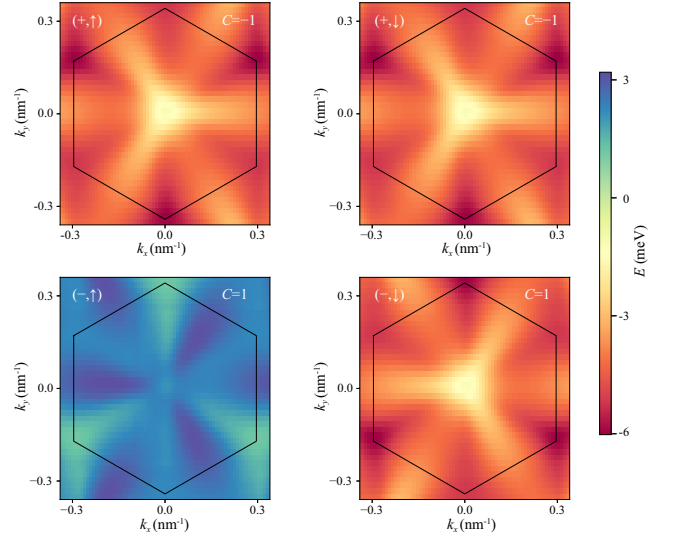


FIG. 3. The four upper fat bands labeled by the valley-spin index (τ, s) are shown for the insulating valley-spin-polarized state obtained from the Hatree-Fock approximation. The Chern numbers of the flat bands are displayed. The black hexagon encloses the moiré BZ.

where λ_s denotes the Lagrange multiplier for the current with spin s and along the α direction, $s_z = \pm 1/2$ is the spin quantum number, and B represents the perpendicular magnetic field. $M_{k,\tau}$ is the orbital magnetic moment

$$M_{k,\tau} = -i \frac{e}{2\hbar} \langle \nabla_k \psi_{k,\tau} | \times (H_{k,\tau} - \varepsilon_{k,\tau}) | \nabla_k \psi_{k,\tau} \rangle \cdot \hat{e}_z, \quad (9)$$

generated by the self rotation of Bloch states [79]. The orbital magnetic moment is spin-degenerate and valley-contrasting. Thus the symmetry breaking state at 3/4 filling has the polarized orbital magnetic moment, and exhibits orbital ferromagnetism. To be concrete, we focus on the current along the x direction and take the valley-spin-polarized ground state in Fig. 3 as the initial state. Because the flat bands with spin down are fully filled, the current can only be conducted by the spin up bands. Hence we fix $\lambda_\downarrow = 0$ in the following. In this case, the Hatree-Fock approximation yields the self-consistent equation in the same form as Eq. (7) but with the replacement $\varepsilon_{k,\tau} \rightarrow \varepsilon_{k,\tau} - \lambda_s \partial_{k_x} \varepsilon_{k,\tau} - g\mu_B s_z B - M_{k,\tau} B$.

We first focus on the effect of current on VP and Hall conductance in the absence of magnetic field $B = 0$. The analysis in Eq. (2) reveals that the switching of VP by currents is of the first order phase transition, and therefore hysteresis is expected. We sweep the current by changing λ continuously and solve the corresponding self-consistent equations. The results of n_τ , n_s , and G_{xy} at zero temperature as a function of λ are displayed in Figs. 4(a) and 4(b), where the hysteresis behavior of VP and Hall conductance appears as expected. Start with the initial state in Fig. 3 with $n_\tau = 1$ and $G_{xy} = -e^2/h$, and then increase λ , both n_τ and G_{xy} change sign through a sharp jump at a critical λ_c . If we remove the current (by setting $\lambda = 0$) after the jump, the system then relaxes into an insulating state

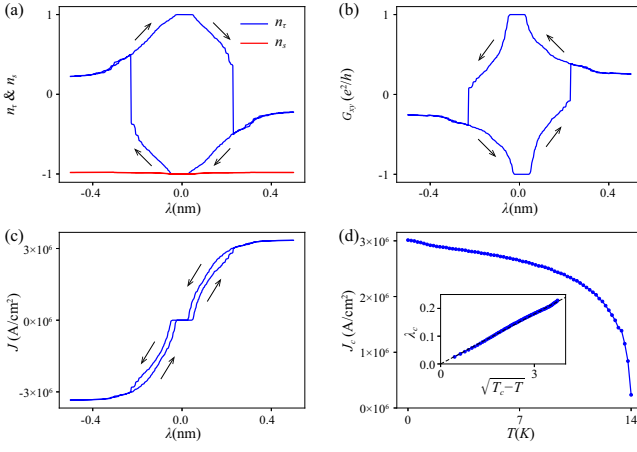


FIG. 4. (a)-(c) Order parameters n_t and n_s , Hall conductance G_{xy} , and current J are plotted as a function of λ , respectively. The arrows indicate the direction of evolution of the hystereses. (d) J_c as a function of T . The inset shows λ_c vs $\sqrt{T_c - T}$.

with $n_t = -1$ and $G_{xy} = e^2/h$, contrary to the initial state [77]. There is no switching of spin polarization because the bands with down spin remain fully occupied.

The current through the TBG is $J = \frac{e}{Ah} \sum_{k,\tau,s} \frac{\partial \epsilon_{k,\tau}}{\hbar \partial k_x} f(E_{k,\tau,s})$, where $h = 0.6$ nm is the thickness of TBG. In Fig. 4(c), we show J as a function of λ . For a small λ , the system remains insulating with $J = 0$, that corresponds to the quantized plateau of $n_t = \pm 1$ in Fig. 4(a) and $G_{xy} = \mp e^2/h$ in Fig. 4(b). As λ increases above a threshold value, the system becomes metallic and there appears hysteresis of J upon increasing and decreasing λ . Eventually, the current saturates at large λ . Our results demonstrate that the VP and topology can be switched by a current larger than the critical current J_c [77].

Here λ_c and J_c are determined by the energy barrier separating different valley-polarized states. As T increases, the energy barrier decreases, and hence λ_c and J_c decreases with T . The dependence of λ_c and J_c on T are shown in Fig. 4(d).

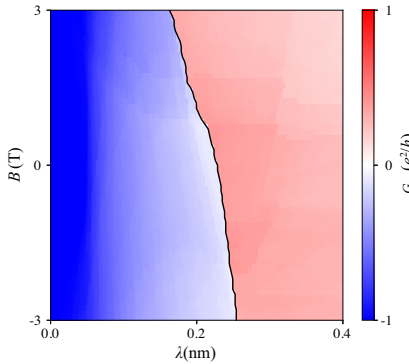


FIG. 5. Density plot of the Hall conductance G_{xy} as a function of λ for different B . The black line corresponds to the critical λ_c as a function of B .

As can be derived from Eq. (2), we have the following scaling relations $\mathcal{F} \sim (T_c - T)^2$, $\delta \sim \sqrt{T_c - T}$, and $\alpha_3 \sim \lambda$. Therefore $\lambda_c \sim \sqrt{T_c - T}$ consistent with the numerical results shown in the inset of Fig. 4(d).

The energy barrier is affected by the magnetic field through the Zeeman coupling with spin and orbital magnetic moments in Eq. (8). In TBG, the orbital magnetic moment is dominant and is valley-contrasting. The energy gap of the insulating valley-spin-polarized state scales linearly with B . To study the dependence of λ_c on B , we show G_{xy} as a function of λ for different B at zero temperature in Fig. 5. The switching of VP and topology at λ_c is featured by the jump of G_{xy} where G_{xy} changes sign. λ_c indicated by the black line in Fig. 5 changes almost linearly with B , which is similar to the gap.

Discussion and summary.— In our approach, only the bulk current contribution is considered. The contribution from edge current relies on the asymmetry of sample edges and can also lift the degeneracy of different valley-spin-polarized ground states. Nevertheless, to switch the VP and topology of TBG, it requires to overcome the bulk energy barrier, which grows linearly with the sample volume. Therefore, the edge current contribution becomes negligible for a large system size [77]. For a small device, it is possible that both the edge and bulk contribution cooperate in the switching process. As in the classical first order phase transition, the transition from one metastable state to the other more stable state occurs via domain nucleation. Our critical current defined when the energy barrier vanishes completely corresponds to the superheating/supercooling field.

In summary, we propose a mechanism of the switching of VP and topology in TBG by bulk electric currents. The current causes the redistribution of electron occupation, that lifts the degeneracy and even overcomes the energy barrier between different valley-spin-polarized states through the Coulomb interaction. Our theory can be generalized to other strongly correlated two dimensional materials with valley polarization.

Acknowledgements.—The authors thank Fengcheng Wu for helpful discussion. Computer resources for numerical calculations were supported by the Institutional Computing Program at LANL. This work was carried out under the auspices of the U.S. DOE NNSA under contract No. 89233218CNA000001 through the LDRD Program, and was supported by the Center for Nonlinear Studies at LANL and Institute for Materials Science (IMS) at LANL through IMS Rapid Response. This work was also supported by the U.S. Department of Energy, Office of Science, Basic Energy Sciences, Materials Sciences and Engineering Division, Condensed Matter Theory Program.

- [1] A. H. Castro Neto, F. Guinea, N. M. R. Peres, K. S. Novoselov, and A. K. Geim, “The electronic properties of graphene,” *Rev. Mod. Phys.* **81**, 109–162 (2009).

- [2] J. M. B. Lopes dos Santos, N. M. R. Peres, and A. H. Castro Neto, “Graphene bilayer with a twist: Electronic structure,” *Phys. Rev. Lett.* **99**, 256802 (2007).
- [3] Rafi Bistritzer and Allan H. MacDonald, “Moiré bands in twisted double-layer graphene,” *PNAS* **108**, 12233–12237 (2011).
- [4] Yuan Cao, Valla Fatemi, Ahmet Demir, Shiang Fang, Spencer L. Tomarken, Jason Y. Luo, Javier D. Sanchez-Yamagishi, Kenji Watanabe, Takashi Taniguchi, Efthimios Kaxiras, Ray C. Ashoori, and Pablo Jarillo-Herrero, “Correlated insulator behaviour at half-filling in magic-angle graphene superlattices,” *Nature* **556**, 80–84 (2018).
- [5] Yuan Cao, Valla Fatemi, Shiang Fang, Kenji Watanabe, Takashi Taniguchi, Efthimios Kaxiras, and Pablo Jarillo-Herrero, “Unconventional superconductivity in magic-angle graphene superlattices,” *Nature* **556**, 43–50 (2018).
- [6] Aaron L. Sharpe, Eli J. Fox, Arthur W. Barnard, Joe Finney, Kenji Watanabe, Takashi Taniguchi, M. A. Kastner, and David Goldhaber-Gordon, “Emergent ferromagnetism near three-quarters filling in twisted bilayer graphene,” *Science* **365**, 605–608 (2019).
- [7] M. Serlin, C. L. Tschirhart, H. Polshyn, Y. Zhang, J. Zhu, K. Watanabe, T. Taniguchi, L. Balents, and A. F. Young, “Intrinsic quantized anomalous hall effect in a moiré heterostructure,” *Science* (2019), 10.1126/science.aay5533.
- [8] Kyoungwan Kim, Ashley DaSilva, Shengqiang Huang, Babak Fallahazad, Stefano Larentis, Takashi Taniguchi, Kenji Watanabe, Brian J. LeRoy, Allan H. MacDonald, and Emanuel Tutuc, “Tunable moiré bands and strong correlations in small-twist-angle bilayer graphene,” *PNAS* **114**, 3364–3369 (2017).
- [9] Shengqiang Huang, Kyoungwan Kim, Dmitry K. Efimkin, Timothy L. L. Lovorn, Takashi Taniguchi, Kenji Watanabe, Allan H. MacDonald, Emanuel Tutuc, and Brian J. LeRoy, “Topologically protected helical states in minimally twisted bilayer graphene,” *Phys. Rev. Lett.* **121**, 037702 (2018).
- [10] Cenke Xu and Leon Balents, “Topological superconductivity in twisted multilayer graphene,” *Phys. Rev. Lett.* **121**, 087001 (2018).
- [11] Hoi Chun Po, Liujun Zou, Ashvin Vishwanath, and T. Senthil, “Origin of mott insulating behavior and superconductivity in twisted bilayer graphene,” *Phys. Rev. X* **8**, 031089 (2018).
- [12] Mikito Koshino, Noah F. Q. Yuan, Takashi Koretsune, Masayuki Ochi, Kazuhiko Kuroki, and Liang Fu, “Maximally localized wannier orbitals and the extended hubbard model for twisted bilayer graphene,” *Phys. Rev. X* **8**, 031087 (2018).
- [13] Jian Kang and Oskar Vafek, “Symmetry, maximally localized wannier states, and a low-energy model for twisted bilayer graphene narrow bands,” *Phys. Rev. X* **8**, 031088 (2018).
- [14] Cheng-Cheng Liu, Li-Da Zhang, Wei-Qiang Chen, and Fan Yang, “Chiral spin density wave and $d + id$ superconductivity in the magic-angle-twisted bilayer graphene,” *Phys. Rev. Lett.* **121**, 217001 (2018).
- [15] J. F. Dodaro, S. A. Kivelson, Y. Schattner, X. Q. Sun, and C. Wang, “Phases of a phenomenological model of twisted bilayer graphene,” *Phys. Rev. B* **98**, 075154 (2018).
- [16] Hiroki Isobe, Noah F. Q. Yuan, and Liang Fu, “Unconventional superconductivity and density waves in twisted bilayer graphene,” *Phys. Rev. X* **8**, 041041 (2018).
- [17] Louk Rademaker and Paula Mellado, “Charge-transfer insulation in twisted bilayer graphene,” *Phys. Rev. B* **98**, 235158 (2018).
- [18] Francisco Guinea and Niels R. Walet, “Electrostatic effects, band distortions, and superconductivity in twisted graphene bilayers,” *Proceedings of the National Academy of Sciences* **115**, 13174–13179 (2018).
- [19] Ming Xie and Allan H. MacDonald, “On the nature of the correlated insulator states in twisted bilayer graphene,” (2018), [arXiv:1812.04213 \[cond-mat.mes-hall\]](https://arxiv.org/abs/1812.04213).
- [20] Matthew Yankowitz, Shaowen Chen, Hryhorii Polshyn, Yuxuan Zhang, K. Watanabe, T. Taniguchi, David Graf, Andrea F. Young, and Cory R. Dean, “Tuning superconductivity in twisted bilayer graphene,” *Science* **363**, 1059–1064 (2019).
- [21] Alexander Kerelsky, Leo J. McGilly, Dante M. Kennes, Lede Xian, Matthew Yankowitz, Shaowen Chen, K. Watanabe, T. Taniguchi, James Hone, Cory Dean, et al., “Maximized electron interactions at the magic angle in twisted bilayer graphene,” *Nature* **572**, 95–100 (2019).
- [22] Yuan Cao, Debanjan Chowdhury, Daniel Rodan-Legrain, Oriol Rubies-Bigorda, Kenji Watanabe, Takashi Taniguchi, T. Senthil, and Pablo Jarillo-Herrero, “Strange metal in magic-angle graphene with near planckian dissipation,” *arXiv preprint arXiv:1901.03710* (2019).
- [23] Hryhorii Polshyn, Matthew Yankowitz, Shaowen Chen, Yuxuan Zhang, K. Watanabe, T. Taniguchi, Cory R. Dean, and Andrea F. Young, “Large linear-in-temperature resistivity in twisted bilayer graphene,” *Nature Physics* **15**, 1011–1016 (2019).
- [24] Guorui Chen, Aaron L. Sharpe, Eli J. Fox, Ya-Hui Zhang, Shaoxin Wang, Lili Jiang, Bosai Lyu, Hongyuan Li, Kenji Watanabe, Takashi Taniguchi, et al., “Tunable correlated Chern insulator and ferromagnetism in trilayer graphene/boron nitride moiré superlattice,” *arXiv preprint arXiv:1905.06535* (2019).
- [25] Emilio Codecido, Qiyue Wang, Ryan Koester, Shi Che, Haidong Tian, Rui Lv, Son Tran, Kenji Watanabe, Takashi Taniguchi, Fan Zhang, Marc Bockrath, and Chun Ning Lau, “Correlated insulating and superconducting states in twisted bilayer graphene below the magic angle,” *Science Advances* **5** (2019), 10.1126/sciadv.aaw9770, <https://advances.sciencemag.org/content/5/9/eaaw9770.full.pdf>.
- [26] Yonglong Xie, Biao Lian, Berthold Jäck, Xiaomeng Liu, Cheng-Li Chiu, Kenji Watanabe, Takashi Taniguchi, B. Andrei Bernevig, and Ali Yazdani, “Spectroscopic signatures of many-body correlations in magic-angle twisted bilayer graphene,” *Nature* **572**, 101–105 (2019).
- [27] Yuhang Jiang, Xinyuan Lai, Kenji Watanabe, Takashi Taniguchi, Kristjan Haule, Jinhai Mao, and Eva Y. Andrei, “Charge order and broken rotational symmetry in magic-angle twisted bilayer graphene,” *Nature* **573**, 91–95 (2019).
- [28] Youngjoon Choi, Jeannette Kemmer, Yang Peng, Alex Thomson, Harpreet Arora, Robert Polski, Yiran Zhang, Hechen Ren, Jason Alicea, Gil Refael, et al., “Electronic correlations in twisted bilayer graphene near the magic angle,” *Nature Physics* **15**, 1174–1180 (2019).
- [29] Xiaobo Lu, Petr Stepanov, Wei Yang, Ming Xie, Mohammed Ali Aamir, Ipsita Das, Carles Urgell, Kenji Watanabe, Takashi Taniguchi, Guangyu Zhang, et al., “Superconductors, orbital magnets and correlated states in magic-angle bilayer graphene,” *Nature* **574**, 653–657 (2019).
- [30] S. L. Tomarken, Y. Cao, A. Demir, K. Watanabe, T. Taniguchi, P. Jarillo-Herrero, and R. C. Ashoori, “Electronic compressibility of magic-angle graphene superlattices,” *Phys. Rev. Lett.* **123**, 046601 (2019).
- [31] Cheng Shen, Na Li, Shuopei Wang, Yanchong Zhao, Jian Tang, Jieying Liu, Jinpeng Tian, Yanbang Chu, Kenji Watanabe, Takashi Taniguchi, et al., “Observation of superconductivity with T_c onset at 12 K in electrically tunable twisted double bilayer graphene,” (2019), [arXiv:1903.06952 \[cond-mat.mes-hall\]](https://arxiv.org/abs/1903.06952).
- [32] Xiaomeng Liu, Zeyu Hao, Eslam Khalaf, Jong Yeon Lee, Kenji

- Watanabe, Takashi Taniguchi, Ashvin Vishwanath, and Philip Kim, “Spin-polarized correlated insulator and superconductor in twisted double bilayer graphene,” (2019), [arXiv:1910.04654 \[cond-mat.mes-hall\]](#).
- [33] Yuan Cao, Daniel Rodan-Legrain, Oriol Rubies-Bigordà, Jeong Min Park, Kenji Watanabe, Takashi Taniguchi, and Pablo Jarillo-Herrero, “Electric field tunable correlated states and magnetic phase transitions in twisted bilayer-bilayer graphene,” (2019), [arXiv:1903.08596 \[cond-mat.mes-hall\]](#).
- [34] Yi-Zhuang You and Ashvin Vishwanath, “Superconductivity from valley fluctuations and approximate $so(4)$ symmetry in a weak coupling theory of twisted bilayer graphene,” *npj Quantum Materials* **4**, 1–12 (2019).
- [35] Qing-Kun Tang, Lin Yang, Da Wang, Fu-Chun Zhang, and Qiang-Hua Wang, “Spin-triplet f -wave pairing in twisted bilayer graphene near $\frac{1}{4}$ -filling,” *Phys. Rev. B* **99**, 094521 (2019).
- [36] J. González and T. Stauber, “Kohn-luttinger superconductivity in twisted bilayer graphene,” *Phys. Rev. Lett.* **122**, 026801 (2019).
- [37] Ying Su and Shi-Zeng Lin, “Pairing symmetry and spontaneous vortex-antivortex lattice in superconducting twisted-bilayer graphene: Bogoliubov-de gennes approach,” *Phys. Rev. B* **98**, 195101 (2018).
- [38] Aline Ramires and Jose L. Lado, “Electrically tunable gauge fields in tiny-angle twisted bilayer graphene,” *Phys. Rev. Lett.* **121**, 146801 (2018).
- [39] Grigory Tarnopolsky, Alex Jura Kruchkov, and Ashvin Vishwanath, “Origin of magic angles in twisted bilayer graphene,” *Phys. Rev. Lett.* **122**, 106405 (2019).
- [40] Junyeong Ahn, Sungjoon Park, and Bohm-Jung Yang, “Failure of nielsen-ninomiya theorem and fragile topology in two-dimensional systems with space-time inversion symmetry: Application to twisted bilayer graphene at magic angle,” *Phys. Rev. X* **9**, 021013 (2019).
- [41] Zhida Song, Zhijun Wang, Wujun Shi, Gang Li, Chen Fang, and B. Andrei Bernevig, “All magic angles in twisted bilayer graphene are topological,” *Phys. Rev. Lett.* **123**, 036401 (2019).
- [42] Kasra Hejazi, Chunxiao Liu, Hassan Shapourian, Xiao Chen, and Leon Balents, “Multiple topological transitions in twisted bilayer graphene near the first magic angle,” *Phys. Rev. B* **99**, 035111 (2019).
- [43] Yury Sherkunov and Joseph J. Betouras, “Electronic phases in twisted bilayer graphene at magic angles as a result of van hove singularities and interactions,” *Phys. Rev. B* **98**, 205151 (2018).
- [44] Jian Kang and Oskar Vafeek, “Strong coupling phases of partially filled twisted bilayer graphene narrow bands,” *Phys. Rev. Lett.* **122**, 246401 (2019).
- [45] Kangjun Seo, Valeri N. Kotov, and Bruno Uchoa, “Ferromagnetic mott state in twisted graphene bilayers at the magic angle,” *Phys. Rev. Lett.* **122**, 246402 (2019).
- [46] Yu-Ping Lin and Rahul M. Nandkishore, “Chiral twist on the high- T_c phase diagram in moiré heterostructures,” *Phys. Rev. B* **100**, 085136 (2019).
- [47] Teemu J. Peltonen, Risto Ojajärvi, and Tero T. Heikkilä, “Mean-field theory for superconductivity in twisted bilayer graphene,” *Phys. Rev. B* **98**, 220504 (2018).
- [48] Wen-Yu He, David Goldhaber-Gordon, and K. T. Law, “Giant Orbital Magneto-electric effect and Current-driven Magnetization Switching in Twisted Bilayer Graphene,” [arXiv:1908.11718 \[cond-mat\]](#) (2019), [arXiv: 1908.11718](#).
- [49] Biao Lian, Zhijun Wang, and B. Andrei Bernevig, “Twisted bilayer graphene: A phonon-driven superconductor,” *Phys. Rev. Lett.* **122**, 257002 (2019).
- [50] Young Woo Choi and Hyoungh Joon Choi, “Strong electron-phonon coupling, electron-hole asymmetry, and nonadiabaticity in magic-angle twisted bilayer graphene,” *Phys. Rev. B* **98**, 241412 (2018).
- [51] Fengcheng Wu, A. H. MacDonald, and Ivar Martin, “Theory of phonon-mediated superconductivity in twisted bilayer graphene,” *Phys. Rev. Lett.* **121**, 257001 (2018).
- [52] Shubhayu Chatterjee, Nick Bultinck, and Michael P Zaletel, “Symmetry breaking and skyrmionic transport in twisted bilayer graphene,” [arXiv preprint arXiv:1908.00986](#) (2019).
- [53] Fengcheng Wu, Euyheon Hwang, and Sankar Das Sarma, “Phonon-induced giant linear-in- T resistivity in magic angle twisted bilayer graphene: Ordinary strangeness and exotic superconductivity,” *Phys. Rev. B* **99**, 165112 (2019).
- [54] Fengcheng Wu, “Topological chiral superconductivity with spontaneous vortices and supercurrent in twisted bilayer graphene,” *Phys. Rev. B* **99**, 195114 (2019).
- [55] Fengcheng Wu and Sankar Das Sarma, “Identification of superconducting pairing symmetry in twisted bilayer graphene using in-plane magnetic field and strain,” *Phys. Rev. B* **99**, 220507 (2019).
- [56] Fengcheng Wu and Sankar Das Sarma, “Ferromagnetism and superconductivity in twisted double bilayer graphene,” [arXiv preprint arXiv:1906.07302](#) (2019).
- [57] Ya-Hui Zhang, Dan Mao, Yuan Cao, Pablo Jarillo-Herrero, and T. Senthil, “Nearly flat chern bands in moiré superlattices,” *Phys. Rev. B* **99**, 075127 (2019).
- [58] Bheema Lingam Chittari, Guorui Chen, Yuanbo Zhang, Feng Wang, and Jeil Jung, “Gate-tunable topological flat bands in trilayer graphene boron-nitride moiré superlattices,” *Phys. Rev. Lett.* **122**, 016401 (2019).
- [59] Jong Yeon Lee, Eslam Khalaf, Shang Liu, Xiaomeng Liu, Zeyu Hao, Philip Kim, and Ashvin Vishwanath, “Theory of correlated insulating behaviour and spin-triplet superconductivity in twisted double bilayer graphene,” *Nature communications* **10**, 1–10 (2019).
- [60] Xiao-Chuan Wu, Anna Keselman, Chao-Ming Jian, Kelly Ann Pawlak, and Cenke Xu, “Ferromagnetism and spin-valley liquid states in moiré correlated insulators,” *Phys. Rev. B* **100**, 024421 (2019).
- [61] Tamaghna Hazra, Nishchhal Verma, and Mohit Randeria, “Bounds on the superconducting transition temperature: Applications to twisted bilayer graphene and cold atoms,” *Phys. Rev. X* **9**, 031049 (2019).
- [62] Fang Xie, Zhida Song, Biao Lian, and B Andrei Bernevig, “Topology-bounded superfluid weight in twisted bilayer graphene,” [arXiv preprint arXiv:1906.02213](#) (2019).
- [63] Aleksii Julku, Teemu J Peltonen, Long Liang, Tero T Heikkilä, and Päivi Törmä, “Superfluid weight and berezinskii-kosterlitz-thouless transition temperature of twisted bilayer graphene,” [arXiv preprint arXiv:1906.06313](#) (2019).
- [64] Xiang Hu, Timo Hyart, Dmitry I. Pikulin, and Enrico Rossi, “Geometric and conventional contribution to the superfluid weight in twisted bilayer graphene,” *Phys. Rev. Lett.* **123**, 237002 (2019).
- [65] Jianpeng Liu and Xi Dai, “Anomalous hall effect, magneto-optical properties, and nonlinear optical properties of twisted graphene systems,” [arXiv preprint arXiv:1907.08932](#) (2019).
- [66] Yu Saito, Jingyuan Ge, Kenji Watanabe, Takashi Taniguchi, and Andrea F Young, “Decoupling superconductivity and correlated insulators in twisted bilayer graphene,” (2019), [arXiv:1911.13302 \[cond-mat.mes-hall\]](#).
- [67] Ya-Ning Ren, Chen Lu, Yu Zhang, Si-Yu Li, Yi-Wen Liu, Chao Yan, Zi-Han Guo, Cheng-Cheng Liu, Fan Yang, and Lin He, “Spectroscopic evidence for a spin and valley polarized metallic

- state in a non-magic-angle twisted bilayer graphene,” (2019), [arXiv:1912.07229 \[cond-mat.mes-hall\]](#).
- [68] Si-Yu Li, Yu Zhang, Ya-Ning Ren, Jianpeng Liu, Xi Dai, and Lin He, “Experimental evidence for orbital magnetic moments generated by moiré-scale current loops in twisted bilayer graphene,” arXiv preprint arXiv:1912.13133 (2019).
- [69] Ya-Hui Zhang, Dan Mao, and T. Senthil, “Twisted bilayer graphene aligned with hexagonal boron nitride: Anomalous hall effect and a lattice model,” *Phys. Rev. Research* **1**, 033126 (2019).
- [70] Nick Bultinck, Shubhayu Chatterjee, and Michael P Zaletel, “Anomalous hall ferromagnetism in twisted bilayer graphene,” (2019), [arXiv:1901.08110 \[cond-mat.mes-hall\]](#).
- [71] Jianpeng Liu, Zhen Ma, Jinhua Gao, and Xi Dai, “Quantum valley hall effect, orbital magnetism, and anomalous hall effect in twisted multilayer graphene systems,” *Phys. Rev. X* **9**, 031021 (2019).
- [72] Fengcheng Wu and Sankar Das Sarma, “Collective excitations of quantum anomalous hall ferromagnets in twisted bilayer graphene,” *Phys. Rev. Lett.* **124**, 046403 (2020).
- [73] Manato Fujimoto, Henri Koschke, and Mikito Koshino, “Topological charge pumping by a sliding moiré pattern,” *Phys. Rev. B* **101**, 041112 (2020).
- [74] Ying Su and Shi-Zeng Lin, “Topological sliding moiré heterostructure,” *Phys. Rev. B* **101**, 041113 (2020).
- [75] Yinhan Zhang, Yang Gao, and Di Xiao, “Topological charge pumping in twisted bilayer graphene,” *Phys. Rev. B* **101**, 041410 (2020).
- [76] Jihang Zhu, Jung-Jung Su, and Allan H MacDonald, “The curious magnetic properties of orbital chern insulators,” (2020), [arXiv:2001.05084 \[cond-mat.mes-hall\]](#).
- [77] See Supplemental Materials for (a) the explicit calculation of the toy model and (b) the switching of valley polarization by a pulsed current.
- [78] N. D. Mermin and H. Wagner, “Absence of ferromagnetism or antiferromagnetism in one- or two-dimensional isotropic heisenberg models,” *Phys. Rev. Lett.* **17**, 1133–1136 (1966).
- [79] Ming-Che Chang and Qian Niu, “Berry phase, hyperorbits, and the hofstadter spectrum: Semiclassical dynamics in magnetic bloch bands,” *Phys. Rev. B* **53**, 7010–7023 (1996).
-

Supplemental Material: Switching of valley polarization and topology in twisted bilayer graphene by electric currents

EXPLICIT CALCULATION OF THE TOY MODEL

Here we provide explicit calculation of the toy model using the dispersion relation $\varepsilon_{k,-} = \cos(2k + \pi) - \mu$ for $-\pi \leq k \leq -\pi/2$ and $\varepsilon_{k,-} = \cos[\frac{2}{3}(k + \pi/2)] - \mu$ for $-\pi/2 \leq k \leq \pi$, and $\varepsilon_{k,+} = \varepsilon_{-k,-}$. The results for Δ_{\pm} and current J as a function of λ are displayed in Fig. S1. The switching of VP occurs only for a positive λ because we start with the initial state shown in Fig. 1(a). For $V = 3$ and $\mu = 1.5$, the switching of VP (featured by the crossing of Δ_{\pm}) happens simultaneously with the insulator-to-metal transition, as shown in Figs. S1(a) and S1(b). When the gap is increased by choosing $V = 5$, the system first becomes a metal, and then switches the VP upon further increasing λ , see Figs. S1(c) and S1(d).

The free energy of the system is

$$\mathcal{F} = -k_B T \sum_{k,\tau} \ln [1 + \exp(-E_{k,\tau}/k_B T)] - \frac{\Delta_+ \Delta_-}{V}. \quad (\text{S1})$$

When the VP order parameter $\delta = (\Delta_+ - \Delta_-)/2$ is small, we can expand \mathcal{F} in terms of δ as shown in Eq. (2). The coefficients are

$$\mathcal{F}_0 = -k_B T \sum_{k,\tau} \ln [1 + \exp[-(\varepsilon_{k,\tau} - \lambda \partial_k \varepsilon_{k,\tau} + \rho)/k_B T]] - \frac{\rho^2}{V}, \quad (\text{S2})$$

$$\alpha_1 = - \sum_{k,\tau} \frac{\tau}{1 + \exp(g)}, \quad (\text{S3})$$

$$\alpha_2 = -\frac{1}{2} \sum_{k,\tau} \frac{1}{2k_B T + 2k_B T \cosh(g)} + \frac{1}{V}, \quad (\text{S4})$$

$$\alpha_3 = -\frac{1}{6} \sum_{k,\tau} \frac{2\tau \cosh^3(g) \sinh^4(g/2)}{k_B^2 T^2}, \quad (\text{S5})$$

$$\alpha_4 = -\frac{1}{24} \sum_{k,\tau} \frac{[-2 + \cosh(g)] \text{sech}^4(g/2)}{8k_B^3 T^3}, \quad (\text{S6})$$

with $\rho = (\Delta_+ + \Delta_-)/2$ and $g = (\varepsilon_{k,\tau} - \lambda \partial_k \varepsilon_{k,\tau} + \rho)/k_B T$. In the absence of current $\lambda = 0$, $\alpha_1 = \alpha_3 = 0$ as required by the Z_2 symmetry associated with the VP. One can show explicitly that $\alpha_{1,3}(\lambda) = -\alpha_{1,3}(-\lambda)$ and $\alpha_{2,4}(\lambda) = \alpha_{2,4}(-\lambda)$.

The free energy as a function of δ for different λ and with $V = 3$ and $\mu = 1.5$ is shown in Fig. S2. The presence of a nonzero λ lifts the degeneracy between the two valley-polarized states. As a consequence, one valley-polarized state becomes metastable, while the other becomes the global ground state. Upon further increasing or decreasing λ , the metastable state becomes unstable and the switching of VP happens.

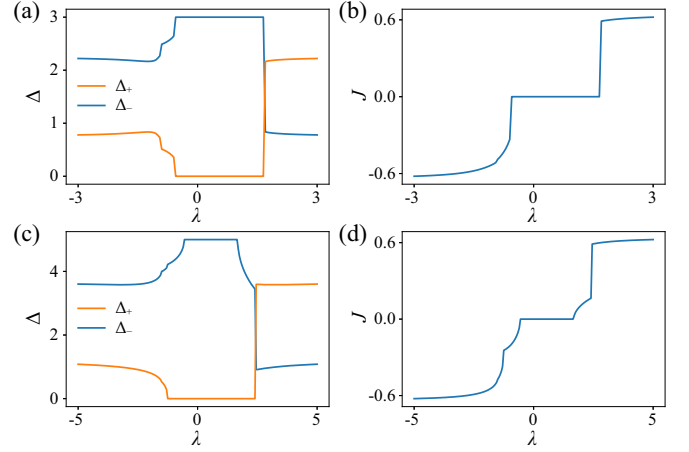


FIG. S1. (a) and (c) Δ_{\pm} as a function of λ for $V = 3$ and 5. The corresponding current J are shown in (b) and (d), respectively.

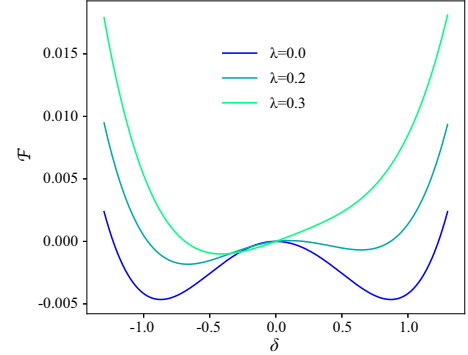


FIG. S2. Free energy as a function of δ for different λ and $V = 3$.

SWITCHING OF VALLEY POLARIZATION BY A PULSED CURRENT

Here we show how the valley polarization is switched by a pulsed current. We assume that the duration of the pulse is much longer than the time scale of electronic relaxation, such that electrons are in a stationary state under the current. We consider three pulsed currents whose peak values are $J_0 = 3.2 \times 10^6$ A/cm², 1.4×10^6 A/cm², and -3.2×10^6 A/cm², respectively, as shown in the upper panel of Fig. S3. The critical current for the switching of VP in this case is $J_c \approx 3 \times 10^6$ A/cm² at zero temperature. The corresponding Hall conductance for the three currents are shown in the lower panel of Fig. S3. Apparently, after the pulse passing, only the Hall conductance for $J_0 = 3.2 \times 10^6$ A/cm² $> J_c$ is flipped from $-e^2/h$ to e^2/h , that indicates the switching of VP and Chern number. For $J_0 = 1.4 \times 10^6$ A/cm² $< J_c$ and for $J_0 = -3.2 \times 10^6$ A/cm² in the opposite direction, there is no switching of valley

polarization as expected.

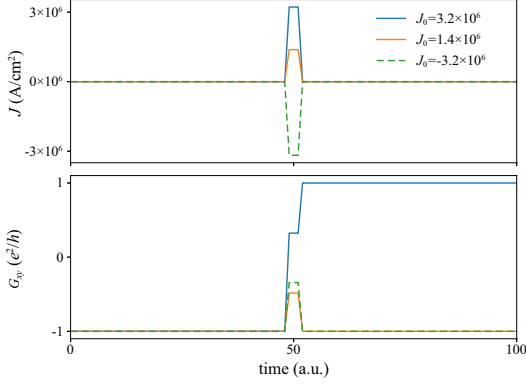


FIG. S3. Upper panel: three pulse currents whose peak values are $J_0 = 3.2 \times 10^6$ A/cm², 1.4×10^6 A/cm², and -3.2×10^6 A/cm², respectively. Lower panel: the corresponding Hall conductance for the three pulsed currents.

ESTIMATE THE EDGE CURRENT CONTRIBUTION IN OVERCOMING THE ENERGY BARRIER

Here we estimate the edge current contribution in overcoming the energy barrier between different ground states with opposite VP. Because of the large unit cell size at a small twist angle, it is hard to access the edge states of the TBG. Instead, we use the edge states of the Haldane model to mimic that of TBG. Explicitly, we consider the Haldane model described by the Hamiltonian [S1]

$$\begin{aligned} \mathcal{H}_H = & 2t_2 \cos \phi \sum_{i=1}^3 \cos(\mathbf{k} \cdot \mathbf{b}_i) \sigma_0 \\ & + t_1 \sum_{i=1}^3 [\cos(\mathbf{k} \cdot \mathbf{a}_i) \sigma_x + \sin(\mathbf{k} \cdot \mathbf{a}_i) \sigma_y] \\ & + \left[M - 2t_2 \sin \phi \sum_{i=1}^3 \sin(\mathbf{k} \cdot \mathbf{b}_i) \right] \sigma_z, \end{aligned} \quad (\text{S7})$$

on a honeycomb lattice whose lattice constant is set to unity. Here t_n is the hopping energy between the n th nearest neighboring (NN) lattice sites, σ_0 is the 2×2 identity matrix, and $\sigma_{x,y,z}$ are the Pauli matrices acting on the sublattice degree of freedom. $\mathbf{a}_{1,2,3}$ are the three vectors connecting NN lattice sites, and $\mathbf{b}_{1,2,3}$ are primitive lattice vectors related by 3-fold rotation. M is the sublattice potential breaking the inversion symmetry, and ϕ is the phase factor associated with the second NN hopping. The topological phase of the model is determined by M and ϕ , as shown by the phase diagram in Fig. S4(a). By choosing $t_2 = 0.07t_1$ and $M = 3t_2$, we show the free energy as a function of ϕ of the Haldane model at half filling and zero temperature in Fig. S4(b). Apparently, there are two degenerate energy minimum with opposite Chern number

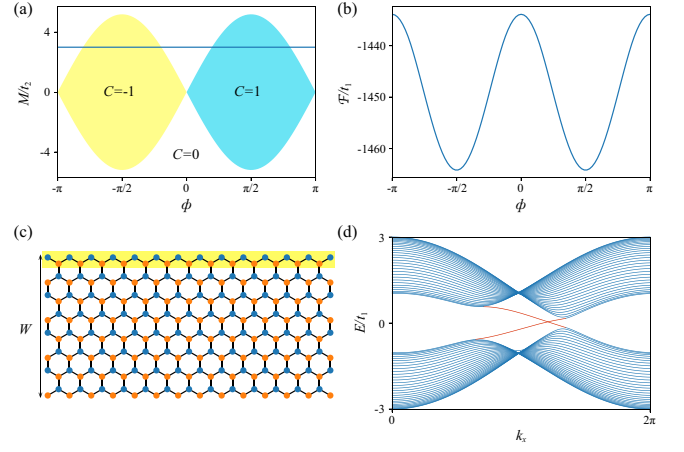


FIG. S4. (a) Phase diagram of the Haldane model. The Chern numbers of different phases are shown. (b) Free energy of the Haldane model along the straight line in (a) at half filling and zero temperature. (c) A strip of honeycomb lattice with width W and zigzag edges. (d) Energy spectrum of the Haldane model on the honeycomb lattice strip.

$C = \pm 1$ at $\phi = \pm\pi/2$, that is similar to the TBG. Therefore, by taking ϕ as an internal order parameter (playing the same role of δ), we can use the Haldane model to mimic the free energy profile and topology of the TBG.

To study the edge current contribution, we consider a stripe of honeycomb lattice with zigzag edges along the x direction, as shown in Fig. S4(c). The edge asymmetry can be introduced by adding an onsite potential V to the upper edge, which is highlighted in Fig. S4(c). For $V = 2t_2$, the energy spectrum of the strip with width $W = 25\sqrt{3}$ (that contains 50 unit cells in the cross section) is shown in Fig. S4(d). Here the edge states traversing the bulk energy gap are marked by red color. In the presence of a current along the strip, the system is described by $\mathcal{H}_H - \sum_n \lambda \partial_{k_x} \epsilon_{k,n}$ where $\epsilon_{k,n}$ represents the bare dispersion of the strip [see Fig. S4(d)] and n is the band index. The current lifts the degeneracy of the two energy minima at $\phi = \pm\pi/2$, as shown in Fig. S5(a). The energy barrier between the two minima vanishes at a critical λ , i.e. $\lambda_c \approx 1.25$ in this case, that corresponds to the switching of VP and topology in TBG. To show the edge current contribution in overcoming the energy barrier, we study the electron occupation in the conduction and valence bands at $\lambda = \lambda_c$. As a reference, we show the electron occupation in the absence of current for $\lambda = 0$ in Fig. S5(b), where the conduction (valence) bands are fully empty (occupied) at zero temperature. The two branches of counter-propagating edge states are partially filled. In the presence of the critical current for $\lambda = \lambda_c$, the electron occupation is shown in Fig. S5(c). Apparently, the branch of edge states propagating along the current direction is fully filled, while the other branch is empty. Moreover, there are electrons pumped from the valence bands to conduction bands as in the TBG. Namely, the edge current alone is not enough to overcome the energy barrier in this case. The

pumped electrons occupy the the bottom of conduction bands where the density of states is high. Therefore, the bulk current plays a dominant role in overcoming the energy barrier for a large system. The edge current can be important if the sample size is small since the energy barrier grows linearly in the sample volume. However, in experiments [6,7], the device is in micron size, that contains hundreds of moiré unit cells (considering the lattice constant of the small-angle TBG is of the order of 10 nm) in the cross section. This fact motivates us to study the switching of VP and topology in TBG by electric currents in the bulk.

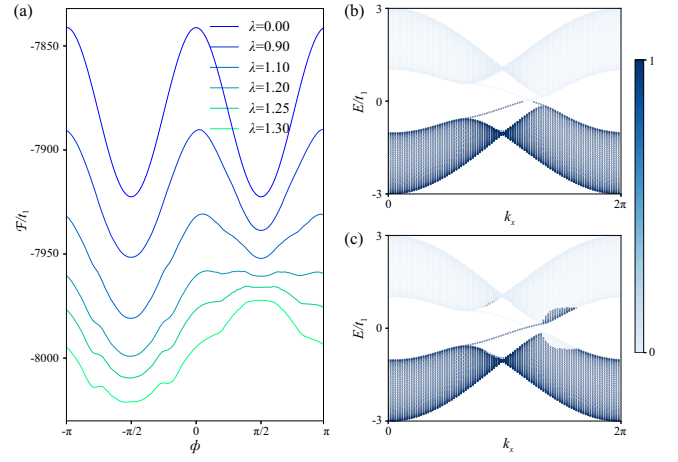


FIG. S5. (a) Free energy of the Haldane model as a function of ϕ for different λ . (b) and (c) Electron occupation for $\lambda = 0$ and for $\lambda = 1.25$, respectively.

[S1] F. D. M. Haldane, Model for a Quantum Hall Effect without Landau Levels: Condensed-Matter Realization of the "Parity Anomaly", Phys. Rev. Lett. **61**, 2015 (1988).